

Coherence resonances on distinct timescales of neural firing

Yu Tong Hu(胡雨桐), Tao Nie(聂涛), Jun Tang(唐军)
Citation: Chin. Phys. B. 35, 098702 (2026). DOI: 10.1088/1674-1056/ae75f8 |
CSTR: 32038.14.CPB.ae75f8
http://cpb.iphy.ac.cn; http://iopscience.iop.org/cpb

What follows is a list of articles you may be interested in

Dynamical behavior analysis for small-world scale-free neural networks

Jieyu Lu(鲁婕妤), Jiapeng Ouyang(欧阳佳鹏), Xue Zhao(赵雪), Minglin Ma(马铭磷)
Chin. Phys. B. 35, 068708 (2026). DOI: 10.1088/1674-1056/ae3609 | CSTR: 32038.14.CPB.ae3609

Anti-interference ability of spiking neuron-astrocyte networks in working memory

Lin Li(李琳), Bingyi Mo(莫冰毅), Shanshan Cheng(程姗姗), Zhouchao Wei(魏周超), Ming Yi(易鸣), Lulu Lu(鹿露露)
Chin. Phys. B. 35, 068703 (2026). DOI: 10.1088/1674-1056/ae4e8c | CSTR: 32038.14.CPB.ae4e8c

Influences of short-term and long-term plasticity of memristive synapse on firing activity of neuronal network

Zhi-Jun Li(李志军), Jing Zhang(张晶)
Chin. Phys. B. 33, 128701 (2024). DOI: 10.1088/1674-1056/ad84c5

Dynamical behavior of memristor-coupled heterogeneous discrete neural networks with synaptic crosstalk

Minglin Ma(马铭磷), Kangling Xiong(熊康灵), Zhijun Li(李志军), Shaobo He(贺少波)
Chin. Phys. B. 33, 028706 (2024). DOI: 10.1088/1674-1056/aceee9

Dynamics and synchronization in a memristor-coupled discrete heterogeneous neuron network considering noise

Xun Yan(晏询), Zhijun Li(李志军), Chunlai Li(李春来)
Chin. Phys. B. 33, 028705 (2024). DOI: 10.1088/1674-1056/ad062c

---

Coherence resonances on distinct timescales of neural firing

Yu-Tong Hu(胡雨桐), Tao Nie(聂涛), and Jun Tang(唐军)†

School of Materials and Physics, China University of Mining and Technology, Xuzhou 221116, *China*

(Received 31 March 2026; revised manuscript received 31 May 2026; accepted manuscript online 2 June 2026)

Coherence resonance (CR) in noise-induced subthreshold neural firings has been extensively studied, and it is well established that neural firing exhibits diverse patterns across multiple timescales. In this study, we partition the neural firings of the Hindmarsh–Rose (HR) neuron model into two distinct timescales — small and large — to investigate coherence resonance at each timescale individually, as well as across the mixed timescales as a whole. Our results show that CR at the smaller timescale emerges primarily when noise-induced firings occur simultaneously at both timescales, whereas CR at the larger and mixed timescales tends to persist over a broader range of parameters. For nonlinear systems possessing multiple markedly disparate timescales, it is methodologically justified to examine their coherence properties separately. These findings provide broader insights into investigating coherence in other nonlinear systems characterized by multiscale dynamics.

Keywords: coherence resonance, neural firing, mixed timescales

PACS: 87.10.–e, 05.40.Ca, 05.70.Fh

DOI: 10.1088/1674-1056/ae75f8 **CSTR:** 32038.14.CPB.ae75f8

1. Introduction

Stochastic resonance (SR) is a well-documented phenomenon observed across a broad range of noisy nonlinear systems, including biological,[1,2] chemical,[3,4] and ecological systems,[5,6] which means that intermediate levels of noise correspond to optimal coherence in a system with input of weak external signals.[7–12] This mechanism facilitates efficient signal transmission and processing in various physical and biological contexts.[13–16] Notably, even in the absence of external signals, noise can induce subthreshold periodic behavior, and moderate noise intensity enables the system to achieve optimal coherence — a phenomenon known as coherence resonance (CR).[17–20] For example, during the release of calcium ions (Ca^{2+}) by a single cluster of 1,4,5-trisphosphate (IP_3) receptors, the periodicity of stochastic calcium signals reaches its maximum when the number of receptors within the cluster is optimal, thereby enabling effective information transmission even under low IP_3 concentrations.[21] In thermoacoustic systems, CR can serve as a signal for the emergence of thermoacoustic instability, allowing researchers to take measures in advance, thus avoiding the effects of instability and prolonging the life of the equipment.[22]

Research on CR in neural systems contributes to a deeper understanding of the pathological mechanisms underlying neurological disorders, thereby providing an evidence-based foundation for their prevention and treatment.[23,24] Consequently, CR in neural systems has been extensively investigated across a variety of neural models.[18,25–30] For instance, the Hodgkin–Huxley (HH) model is a classical spiking neuron model based on the nonlinear conductance of ion channels, which accurately describes action potential firing in real neurons.[29,31–35] The FitzHugh–Nagumo (FHN) model is a simplified version of the HH model and is primarily used to study neural oscillations driven purely by noise.[36,37] The Izhikevich model is an efficient model designed for large-scale neural network simulations.[38] Compared with the FHN model, it offers greater biological plausibility while remaining computationally simpler than the HH model.[38,39]

It is quite common in nonlinear systems for multiple, distinctly different dynamical behaviors to coexist within the same system. Prominent examples include cluster synchronization[40] and chimera states[41] in neural networks, as well as multi-mode oscillations in complex dynamical systems. Despite this prevalence, these coexisting phenomena are rarely analyzed as separate entities within a single system; instead, they are often treated as a unified or averaged collective behavior. Recently, Yang *et al.*[42] proposed an extended master stability function framework to investigate alternating synchronization modes in networked oscillator systems, explicitly treating two distinct synchronous manifolds independently instead of merging or averaging them. Recent studies based on three-dimensional (3D) simplified HH neuron models at multiple timescales have found that white noise can induce different types of firing patterns near subcritical Hopf bifurcations, which has led to the discovery of double stochastic resonances (DCRs), in which the two optimal levels of noise lead to two optimal values of coherence.[43] In the above study, there were two distinct timescales of neural oscillations, and the coherence parameter for the two timescales was not calculated separately. Many experiments have found that neural oscillations

†Corresponding author. E-mail: tjuns1979@126.com

© 2026 Chinese Physical Society and IOP Publishing Ltd. All rights, including for text and data mining, AI training, and similar technologies, are reserved.

have more complex multi-periodic patterns, such as the burst firing simulated by the Hindmarsh–Rose (HR) model.[44,45] In these multi-periodic patterns, more complex CR phenomena may be entailed. In addition, the coherence is measured by calculating the standard deviation of inter-spike intervals (ISIs) in Ref. [43]. However, it is evident that within mixed-mode neural oscillations, there exist at least two distinct timescales of ISIs. The coherence measure is significantly affected by the disparity between the two timescales, thereby drastically diminishing its effectiveness in characterizing the regularity of oscillations. A more appropriate methodology is to compute the standard deviations separately for each distinct timescale.

In this letter, we investigate the CR phenomenon using the HR neuron model, which exhibits richer and more complex oscillatory dynamics compared to simpler neuronal models. The ISIs can be approximately partitioned into two distinct timescales, and the standard deviations of ISIs are then computed separately for each timescale to quantify the regularity of spiking activity and to identify the presence of CR at each timescale independently. This multiscale analysis provides a more precise characterization of ISI variability across different dynamical regimes, thereby offering deeper insight into the intricate dynamical behaviors underlying noise-induced neural firing in systems with multiple intrinsic timescales.

2. Model and simulation

Various neural firing patterns have been observed across different types of neuron cells. The HR model has been one of the most commonly used models to study the nonlinear dynamics of neurons.[44,46,47] The HR neuron model contains three variables: the membrane potential x, the recovery current y, and the slow adaptation current z. It is composed of three nonlinear ordinary differential equations, which are as follows:[48]

$$\begin{aligned}\frac{\mathrm{d}x}{\mathrm{d}t} &= y - ax^3 + bx^2 - z + I_{\mathrm{ext}},\\ \frac{\mathrm{d}y}{\mathrm{d}t} &= c - dx^2 - y,\\ \frac{\mathrm{d}z}{\mathrm{d}t} &= r[s(x - x_0) - z] + D\xi(t).\end{aligned} \tag{1}$$

The parameter values for the HR model are adopted from Ref. [48] and are as follows: $a = 1, b = 3, c = 1, d = 5.0, s = 4, x_0 = -1.6$. Additionally, the values of the parameters r and I_{ext} will be varied according to the specific context of the investigation. Moreover, the additive noise term $D\xi(t)$ is added to the right-hand side of the third equation in Eq. (1) to induce subthreshold neural firing. Here, D denotes the noise intensity, and the statistical properties of the Gaussian white noise are given by

$$\langle \xi(t) \rangle = 0, \quad \langle \xi(t)\xi(t') \rangle = \delta(t - t'), \tag{2}$$

where $\delta(\cdot)$ denotes the Dirac delta function. We use a forward Euler integration scheme with a time step of 10^{-2} time unit. This step size has been verified to ensure numerical convergence throughout the entire parameter regime explored in this study. The numerical algorithm presented by Sancho *et al.*[49] will be used to simulate the noise term. In all simulations, the initial 2000 time units of the trajectory are discarded to eliminate transient effects.

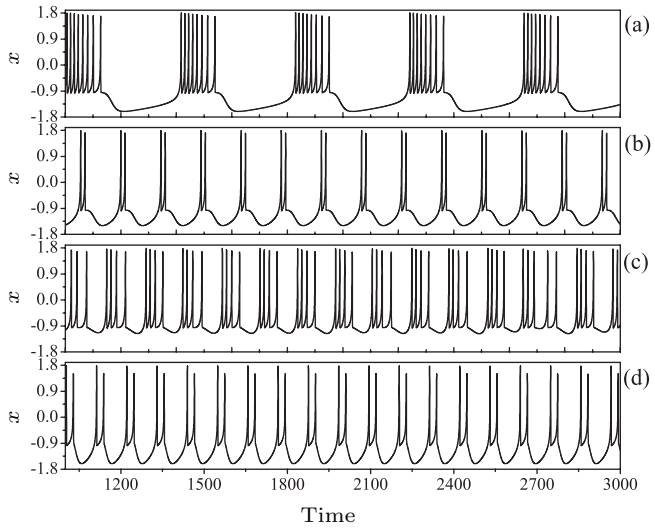


Fig. 1. Typical firing patterns of the HR neural model in the absence of noise ($D = 0.0$). (a) $r = 0.001$, $I_{\mathrm{ext}} = 2.0$, (b) $r = 0.005$, $I_{\mathrm{ext}} = 2.0$, (c) $r = 0.005$, $I_{\mathrm{ext}} = 3.2$, (d) $r = 0.01$, $I_{\mathrm{ext}} = 2.0$.

As illustrated in Fig. 1, the HR model is capable of generating diverse neural firing dynamics, including simple periodic, multi-periodic, and even chaotic oscillations depending on the choice of parameter sets. The inter-spike interval (ISI) is defined as the time elapsed between two consecutive action potentials in a neuronal membrane potential trace.[30,43] The statistical distribution and temporal structure of ISI sequences are instrumental in characterizing neuronal activity patterns. The coefficient of variation of the ISIs is commonly employed to measure the coherence of neuronal firing and is defined as

$$R = \frac{\sqrt{\langle T_i^2 \rangle - \langle T_i \rangle^2}}{\langle T_i \rangle}. \tag{3}$$

Here, T_i denotes the i-th ISI extracted from the membrane potential time series of a single neuron. Throughout this paper, the coherence measure R is computed over 10^8 time units or 4.5×10^4 ISIs. In the low-noise regime, ISIs, particularly small-timescale ISIs, become exceedingly rare. To ensure statistical robustness, the simulation duration is extended until at least 2000 small-timescale ISIs are collected. Owing to the sufficiently long integration times — which yield a large sample size of ISIs — time averaging is employed as a reliable surrogate for ensemble averaging. Consequently, multiple independent realizations under identical parameter settings are not performed. Obviously, a smaller value of R corresponds to higher coherence of the system.

As characterized by the two-parameter (r and $I_{\rm ext}$) bifurcation diagram in Fig. 3 of Ref. [48], the HR model exhibits rich modes of dynamical behavior. For example, the bifurcation diagram of ISI versus $I_{\rm ext}$ for three given values of r ($r = 0.001$, 0.006, and 0.01) is presented in Fig. 2. These bifurcation diagrams are obtained numerically by recording ISIs over a duration of 2×10^4 time units. There exists a critical value of the bifurcation parameter such that when $I_{\rm ext}$ is below this critical value, the neuron remains in a resting state, and only when it exceeds this critical value can the neuron exhibit firing activity. The critical values corresponding to Figs. 2(a)–2(c) are $I_{\rm ext} = 1.27$, 1.36, and 1.43, respectively. Numerical results reveal that, as $I_{\rm ext}$ is varied, the system undergoes complex transitions among single-periodic, multi-periodic, and even chaotic spikes. As illustrated in Figs. 1 and 2, although the HR neuron can exhibit more than two intrinsic timescales in its firing pattern, these timescales can be clearly segregated into two distinct groups that differ substantially from each other. Accordingly, the ISIs are divided into two distinct categories: short-timescale ISIs (sISIs) and long-timescale ISIs (lISIs). The timescale of ISIs exhibits a strong dependence on the parameter r. As r increases, the gap between the sISIs and lISIs narrows significantly, making it highly challenging to select an appropriate critical value to separate them — often requiring reliance on empirical insights from numerical simulations. In this paper, we primarily focus on the parameter range $r < 0.01$. Within this range, any critical value greater than 60 can effectively and clearly separate the two timescales. Based on practical experience from numerical simulations, we specifically choose three critical values — 60, 80, and 100 — to segregate the timescales. It is expected that for $r > 0.01$, the distinction between the two timescales becomes even smaller, making their separation considerably more difficult.

Moreover, it should be emphasized that the aforementioned $I_{\rm ext}$ values correspond to the critical value at which the system transitions from a resting state to the onset of lISIs. We further observe that, as r increases, a higher critical value of $I_{\rm ext}$ is required for the simultaneous emergence of both sISIs and lISIs.

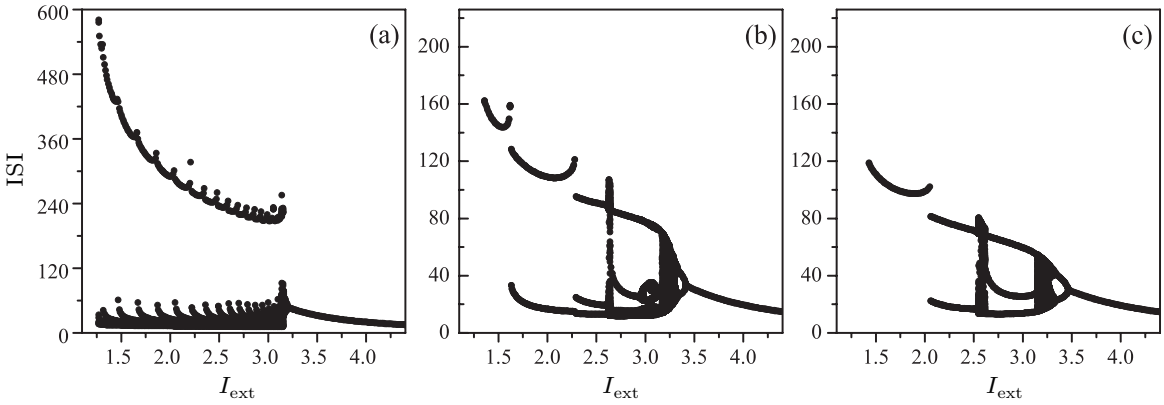


Fig. 2. Bifurcation diagrams of the HR neural model in the absence of noise ($D = 0$), showing the ISI as a function of $I_{\rm ext}$. (a) $r = 0.001$, (b) $r = 0.006$, (c) $r = 0.01$.

3. Results and discussion

3.1. Noise-induced subthreshold firing patterns

CR is a well-documented phenomenon in noise-induced subthreshold oscillatory dynamics. As shown in Fig. 2(a), the HR neuron remains in a resting state for bifurcation parameter $I_{\rm ext} < 1.27$. Therefore, the bifurcation parameter $I_{\rm ext}$ is set to 1.259, and different levels of noise are applied to induce subthreshold neural firing (see Fig. 3). In Fig. 3(a), the weak noise of 7×10^{-8} is insufficient to induce any neural activity. As shown in Figs. 3(b)–3(d), noise can induce mixed-mode neural firing comprising both lISIs and sISIs. Notably, both the firing rate and temporal structure of the neural activity exhibit a pronounced dependence on noise intensity D. In light of the bifurcation diagram in Fig. 2(a), this indicates that different noise levels effectively drive the HR neuron into distinct dynamical regimes.

To clearly illustrate the distinct timescales present in the ISIs, Fig. 4 displays the corresponding probability density functions of the ISIs shown in Fig. 3. At relatively low noise levels, a multimodal distribution in the plot reveals multiple ISI timescales. As the noise intensity D increases, the peaks corresponding to larger timescales gradually merge. Nevertheless, two distinct peaks associated with sISIs and lISIs remain clearly discernible, provided the noise is not excessively high. In contrast to the bimodal distribution reported in Ref. [43], the bimodal peaks observed in this paper are more pronounced, indicating a greater divergence between the two timescales and underscoring the necessity of performing separate statistical analyses of the ISIs at distinct timescales.

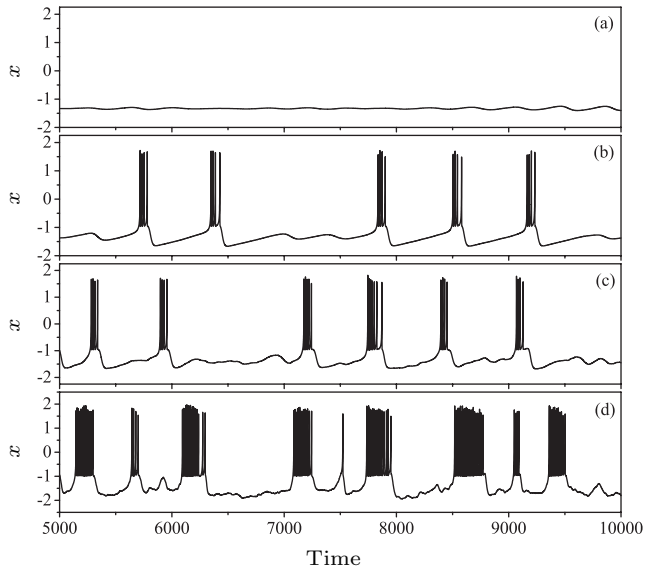


Fig. 3. Noise-induced firing patterns of the HR neural model for $I_{\text{ext}} = 1.259$ and $r = 0.001$ at different noise intensities: (a) $D = 7 \times 10^{-8}$, (b) $D = 2.3 \times 10^{-7}$, (c) $D = 1 \times 10^{-5}$, (d) $D = 0.002$.

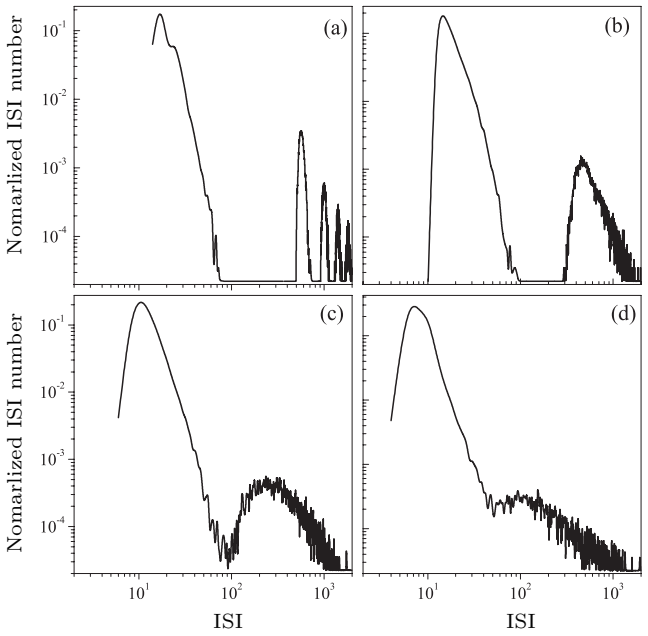


Fig. 4. Probability density of noise-induced ISIs as a function of interval length for $I_{\text{ext}} = 1.259$ and $r = 0.001$ at different noise intensities: (a) $D = 2.3 \times 10^{-7}$, (b) $D = 2 \times 10^{-5}$, (c) $D = 1 \times 10^{-3}$, (d) $D = 1 \times 10^{-2}$.

3.2. Coherence resonance in distinct timescales

To investigate the phenomenon of CR, we compute the coherence measure R across a range of noise intensities. As illustrated in Fig. 4, the ISIs are clearly bimodal and can be unambiguously partitioned into two distinct groups: *s*ISIs and *l*ISIs. A critical value of 100 is adopted to separate *s*ISIs and *l*ISIs. Numerical simulations for $r = 0.001$ indicate that critical values in the range of 80 to 150 appear to yield consistent results, confirming the robustness of the separation. The coherence measure R is calculated separately for *s*ISIs and *l*ISIs, and also for the mixed-timescale ISIs as a whole. Figure 5 shows that valley values exist for both *s*ISIs and *l*ISIs, as well as for all ISIs with mixed timescales. This indicates that CR occurs simultaneously at two distinct timescales.

As shown in Fig. 5, the noise intensities corresponding to optimal coherence are 2.3×10^{-7} for *s*ISIs and 4×10^{-5} for *l*ISIs, differing by nearly two orders of magnitude. This indicates that CR on the small timescale occurs at an exceptionally low noise intensity. In Ref. [43], the coherence measure is significantly distorted by the disparity between two distinct timescales, rendering it incapable of uniquely and quantitatively characterizing oscillation regularity. Consequently, the reported DCR differs substantially from CR in the conventional sense. In contrast, the CR observed in our work — when analyzed separately on each individual timescale — genuinely reflects traditional coherence resonance, as it faithfully captures the regularity of oscillations within each intrinsic dynamical regime.

Notably, Fig. 5(a) reveals a stage-like variation in coherence as a function of noise intensity. This behavior may be qualitatively attributed to the bifurcation structure shown in Fig. 2. Specifically, the *s*ISIs branch in Fig. 2(a) exhibits multiple periodic sub-branches as the bifurcation parameter I_{ext} varies. Different noise intensities effectively shift the system's effective operating point across these sub-branches, thereby modulating the regularity of spiking in a piecewise manner. While this interpretation is consistent with the observed dynamics, more direct and quantitative evidence is required to fully substantiate this mechanism in future work.

To assess the robustness of CR across two distinct timescales, we conducted numerical simulations by varying the bifurcation parameter r. We find that, once r exceeds a certain value, the coherence measure R for *s*ISIs no longer exhibits a minimum; instead, it displays a monotonic, yet stage-like increase with rising noise intensity. As illustrated in Fig. 6(a) for $r = 0.006$, the absence of a valley in R for *s*ISIs clearly indicates the loss of CR. In contrast, the presence of valleys in Figs. 6(b) and 6(c) confirms that CR remains clearly observable for the *l*ISIs and mixed ISIs. It should be noted that at $r = 0.006$, the distinction between the two timescales is already significantly reduced. Numerical simulations suggest that, in this case, a critical value of 80 appears to be a suitable choice for separating the small and large timescales.

As illustrated in Fig. 7, when the noise intensity is 10^{-7}, the weak noise is insufficient to elicit *s*ISIs. *s*ISIs begin to emerge only when the noise intensity increases to 10^{-4}, and their occurrence frequency grows with further increases in D. Notably, CR on the small timescale occurs under extremely low noise conditions ($D \sim 10^{-7}$). However, when the bifurcation parameter r is set to 0.006, such weak noise is inadequate to induce *s*ISIs, thereby preventing the observation of optimal coherence on the small timescale.

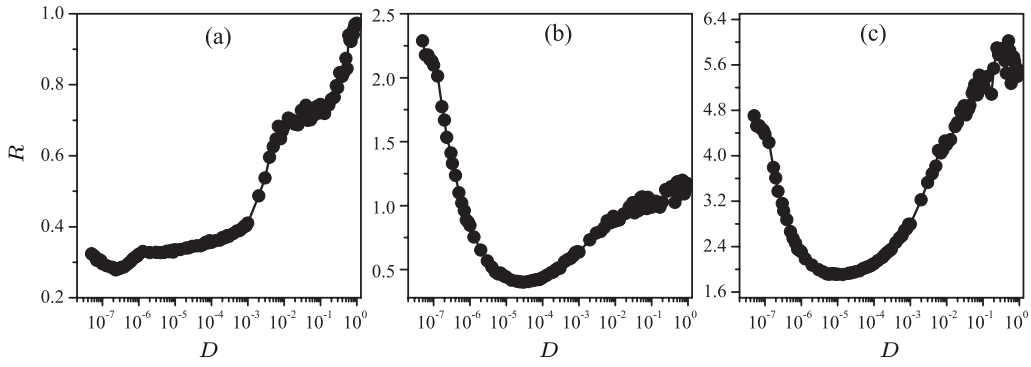


Fig. 5. Coherence measure R as a function of noise intensity D for $I_{\text{ext}} = 1.259$ and $r = 0.001$. A critical value of 100 time units is applied to separate *s*ISIs and *l*ISIs. (a) R computed from *s*ISIs, (b) R computed from *l*ISIs, (c) R computed from the full ISI sequence.

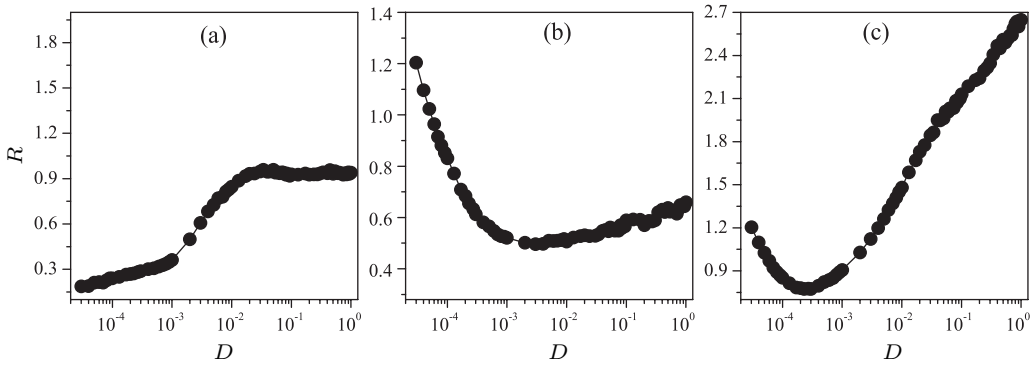


Fig. 6. Coherence measure R as a function of noise intensity D for $I_{\text{ext}} = 1.350$ and $r = 0.006$. A critical value of 80 time units is applied to separate *s*ISIs and *l*ISIs. (a) R computed from *s*ISIs, (b) R computed from *l*ISIs, (c) R computed from the full ISI sequence.

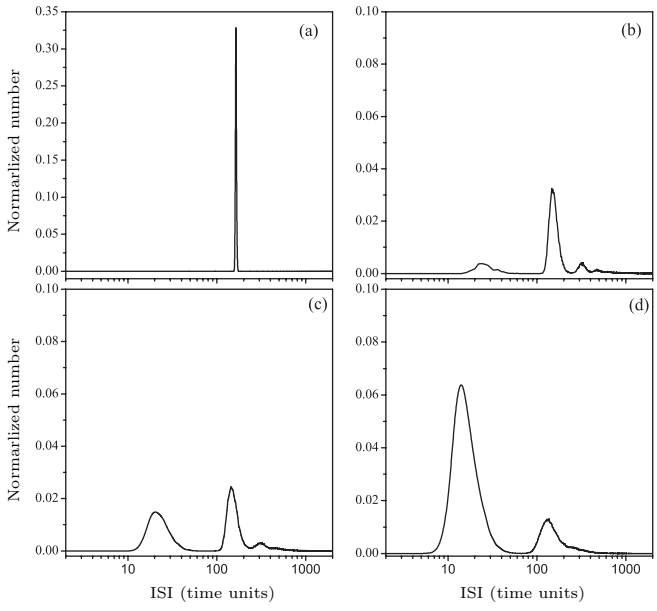


Fig. 7. Probability density of noise-induced ISIs as a function of interval length for $I_{\text{ext}} = 1.35$ and $r = 0.006$ at different noise intensities: (a) $D = 2.3 \times 10^{-7}$, (b) $D = 1 \times 10^{-4}$, (c) $D = 2 \times 10^{-4}$, (d) $D = 1 \times 10^{-3}$.

To understand why weak noise fails to elicit small-timescale spikes, we revisit the bifurcation diagram in Fig. 2. For $r = 0.001$, both *l*ISIs and *s*ISIs emerge simultaneously as I_{ext} crosses the bifurcation value of 1.27. However, when r is increased to 0.006, crossing the first bifurcation value at $I_{\text{ext}} = 1.36$ yields only *l*ISIs. The *s*ISIs appear only after I_{ext} exceeds a second, higher bifurcation value at $I_{\text{ext}} = 1.62$. The bifurcation points for *s*ISIs and *l*ISIs, and the difference between the two bifurcation points, are plotted as a function of r in Fig. 8. For $r \leq 0.003$, the difference between the bifurcation points of *s*ISIs and *l*ISIs is zero, indicating the simultaneous emergence of both *s*ISIs and *l*ISIs once noise triggers subthreshold firing. However, for $r > 0.003$, weak noise is sufficient to drive the neuron across the large-timescale bifurcation point, leading to *l*ISIs, but remains inadequate to cross the small-timescale bifurcation point to generate *s*ISIs.

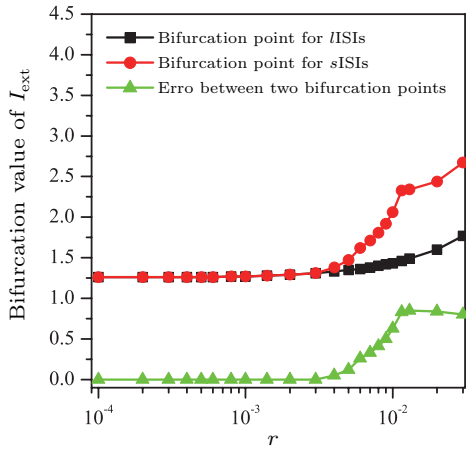


Fig. 8. The bifurcation values of I_{ext} for the onset of *s*ISIs and *l*ISIs as functions of the parameter r. The difference between the two bifurcation values is also shown.

Extensive numerical simulations were conducted within the parameter regime $r < 0.01$, with I_{ext} set close to the bifurcation points and the noise intensity systematically varied

from 10^{-9} to 1. The results suggest that CR in *s*ISIs occurs primarily when noise-induced *s*ISIs and *l*ISIs emerge simultaneously. As r increases, however, the generation of *s*ISIs tends to require higher noise intensities, which may lead to the suppression or absence of CR in this regime. In contrast, CR in the *l*ISIs and mixed ISIs appears to persist more robustly across the parameter range examined.

4. Conclusion

In summary, we investigate the phenomenon of CR in the HR neural model, which is well known to exhibit mixed–mode oscillations. By partitioning the noise-induced subthreshold neural firing into two distinct timescales: *s*ISIs and *l*ISIs, we analyze CR phenomena separately at each timescale. Our results demonstrate that CR at the smaller timescale is highly sensitive to the neural bifurcation behavior and vanishes when the bifurcation values for *s*ISIs and *l*ISIs diverge. In contrast, CR appears to persist more robustly at the larger and mixed timescales. Given that mixed-mode oscillations are ubiquitous in a wide range of nonlinear systems,[50–53] our multiscale approach to dissecting coherence resonance offers not only deeper insight into neural dynamics but also a general framework applicable to the study of noise-induced subthreshold oscillations in multiscale nonlinear systems.

References

[1] van der Groen O, Tang M F, Wenderoth N and Mattingley J B 2018 *PLoS Comput. Biol.* **14** e1006301
[2] McDonnell M D and Abbott D 2009 *PLoS Comput. Biol.* **5** e1000348
[3] Ke Y L 2025 *J. Chem. Phys.* **162** 064702
[4] Zeyer K P, Mäinster A F and Gilles E D 2002 *Phys. Chem. Chem. Phys.* **4** 5988
[5] Park J I, Kim B J and Park H J 2021 *Phys. Rev. E* **104** 024133
[6] Rozenfeld A F, Tessone C J, Albano E and Wio H S 2001 *Phys. Lett. A* **280** 45
[7] Budrikis Z 2021 *Nat. Rev. Phys.* **3** 771
[8] Dykman M I and McClintock P V E 1998 *Nature* **391** 344
[9] Gammaitoni L, Hänggi P, Jung P and Marchesoni F 1998 *Rev. Mod. Phys.* **70** 223
[10] Liang Q, Yu W X and Xiao Q M 2025 *Chin. Phys. B* **34** 040502
[11] Li X, Nie D, Xu M and Zhang K 2025 *Chin. Phys. B* **34** 050203
[12] Jin Y F, Wang H T and Zhang T T 2024 *Chin. Phys. B* **33** 010501
[13] Gammaitoni L, Hänggi P, Jung P and Marchesoni F 2009 *Eur. Phys. J. B* **69** 1
[14] Itzcovich E, Riani M and Sannita W G 2017 *Sci. Rep.* **7** 12840
[15] Fu Y X, Kang Y M and Chen G R 2020 *Front. Comput. Neurosci.* **14** 24
[16] Yamazaki H and Lioumis P 2022 *Neuropsychologia* **168** 108174
[17] Pikovsky A S and Kurths J 1997 *Phys. Rev. Lett.* **78** 775
[18] Pradines J R, Osipov G V and Collins J J 1999 *Phys. Rev. E* **60** 6407
[19] Perc M 2005 *Phys. Rev. E* **72** 016207
[20] Bogatenko T R and Semenov V V 2018 *Phys. Lett. A* **382** 2645
[21] Shuai J W and Jung P 2002 *Phys. Rev. Lett.* **88** 068102
[22] Kabiraj L, Steinert R, Saurabh A and Paschereit C O 2015 *Phys. Rev. E* **92** 042909
[23] Kim J H, Lee H J, Min C H and Lee K J 2015 *Phys. Rev. E* **92** 042701
[24] Ma J and Tang J 2017 *Nonlinear Dyn.* **89** 1569
[25] Lindner B, García-Ojalvo J, Neiman A and Schimansky-Geier L 2004 *Phys. Rep.* **392** 321
[26] Pisarchik A N and Hramov A E 2023 *Phys. Rep.* **1000** 1
[27] Hu Y and Tang J 2025 *Eur. Phys. J. Spec. Top.* **234** 8873
[28] Tang J, Zhang J, Ma J and Luo J M 2019 *Sci. China Tech. Sci.* **62** 1134
[29] Tang J, Liu T B, Ma J, Luo J M and Yang X Q 2016 *Comm. Nonlinear Sci. Numer. Simul.* **32** 262
[30] Tang J, Jia Y, Yi M, Ma J and Li J R 2008 *Phys. Rev. E* **77** 061905
[31] Goldwyn J H, Imennov N S, Famulare M and Shea-Brown E 2011 *Phys. Rev. E* **83** 041908
[32] Hashemi M, Valizadeh A and Azizi Y 2012 *Phys. Rev. E* **85** 021917
[33] Ullah G and Schiff S J 2009 *Phys. Rev. E* **79** 040901
[34] Hodgkin A L and Huxley A F 1990 *Bull. Math. Biol.* **52** 25
[35] Peng L, Tang J, Ma J and Luo J M 2022 *Physica A* **594** 126956
[36] Manchein C, Santana L, da Silva R M and Beims M W 2022 *Chaos* **32** 083102
[37] Cubero D, Baltanás J P and Casado-Pascual J 2006 *Phys. Rev. E* **73** 061102
[38] Izhikevich E M 2003 *IEEE Trans. Neural Netw.* **14** 1569
[39] Izhikevich E M 2004 *IEEE Trans. Neural Netw.* **15** 1063
[40] Blaha K A, Huang K, Rossa F D, Pecora L, Hossein-Zadeh M and Sorrentino F 2019 *Phys. Rev. Lett.* **122** 014101
[41] Zhang H, Chen Z, Liu F, Lei Z, Zheng Z and Qian Y 2024 *New J. Phys.* **26** 023016
[42] Yang R, Wang Y, Wang X, Lei Z, Zheng Z and Qian Y 2026 *New J. Phys.* **28** 013901
[43] Li L and Zhao Z 2022 *Phys. Rev. E* **105** 034408
[44] Hindmarsh J L and Rose R M 1984 *Proc. R. Soc. Lond. B* **221** 87
[45] Shi X and Wang Z 2020 *Neural Plast.* **2020** 8826369
[46] Izhikevich E M 2000 *Int. J. Bifurcation Chaos* **10** 1171
[47] Rothkegel A and Lehnertz K 2014 *New J. Phys.* **16** 055006
[48] Gu H 2013 *PLoS One* **8** e81759
[49] Sancho J M, San Miguel M, Katz S L and Gunton J D 1982 *Phys. Rev. A* **26** 1589
[50] Jalicsa J, Krupa M and Rotstein H G 2010 *Dyn. Sys.* **25** 445
[51] Medvedeva G S and Cisternas J E 2004 *Phys. D* **194** 333
[52] Liu P, Liu X and Yu P 2017 *Commun. Nonlinear Sci. Numer. Simul.* **52** 148
[53] Ghaffari B, Kouhnavard M and Elbasiouny S M 2016 *PLoS One* **12** e0178244